Combustion Cycle-To-Cycle Variation Analysis in Diesel Baseline Hydrogen-Fueled Spark-Ignition Engines

Caio Ramalho Leite, Richard Oung, Pierre Brequigny, Jacques Borée, Fabrice Foucher

Combustion cycle-to-cycle variation analysis in diesel baseline hydrogen-fueled spark-ignition engines

Caio Ramalho Leite, Richard Oung, Pierre Brequigny
Université d'Orléans, France

Jacques Borée
ENSMA, France

Fabrice Foucher
Université d'Orléans, France

ABSTRACT

In the search for zero-carbon emissions and energy supply security, hydrogen is one of the fuels considered for internal combustion engines. The state-of-the-art studies show that a good strategy to mitigate NOx emissions in hydrogen-fueled spark-ignition engines (H2ICE) is burning ultra-lean hydrogen-air mixtures in current diesel architectures, due to their capability of standing high in-cylinder pressures. However, it is well-known that decreasing equivalence ratio leads to higher engine instability and greater cycle-to-cycle variations (CCVs). Nevertheless, hydrogen flames, especially at low equivalence ratios and high pressures, present thermodiffusive instabilities that speed up combustion, changing significantly the flame development and possibly its variability. This work evaluates the hydrogen combustion and their CCVs in two single-cylinder diesel baseline H2ICEs (light-duty and medium-duty) and their influence on performance parameters. The analysis is done using three CCV indicators (for flame initiation, propagation, and end-flame periods) in four main strategies: varying fuel-air equivalence ratio (from 0.2 to 0.8), swirl intensity, spark timing, and spark plug type. The cyclic variations are higher at low loads and leaner mixtures. While, at high loads, the engine presents low combustion CCVs, around 10 % in all combustion phases, at idle they can go up to 20 % in the flame propagation phase (10 to 50 % of mass fraction burned - MFB). The fluctuations of the flame propagation duration are highly impacted by the equivalence ratio. Furthermore, the behavior of the combustion duration at the initiation (0 to 10 % MFB) and propagation phases suggests that other phenomena play an important role in hydrogen combustion in engines besides the laminar burning velocity property. For this, a flame speed enhancement model which considers hydrogen's intrinsic instabilities is applied to evaluate the flames at the operating conditions.

INTRODUCTION

As a response to the threat posed by climate change [1] and the concern of energy supply security [2, 3, 4], hydrogen takes an important and strategic place as a future energy carrier, particularly concerning the transport industry. For this, green hydrogen is considered one of the future fuels in internal combustion engines (ICEs) [4].

Hydrogen-fueled spark-ignition internal combustion engines (H_2ICEs) can be used with two main strategies: (1) close-to-stoichiometric, and (2) low fuel-air equivalence ratio (ϕ). For the first one, the H_2/air mixture at stoichiometry leads to higher flame speeds, higher power, and lower cyclic variations, but higher flame temperature and NOx emissions. For the second one, lean hydrogen mixtures have not only lower flame temperature and NOx emissions, but also lower flame speed and higher cyclic variations [4].

Aiming to reduce pollutants emissions and increase the engine's efficiency, cyclic variability is one of the major study subjects concerning highly optimized ICEs [5]. Ozdor et al.'s review [6] suggests that the elimination of cycle-to-cycle variations (CCVs) could lead to a 10 % increase in the engine power output for the same fuel consumption. It is well known that CCVs are the result of alterations in the combustion process and can be caused by the disparity of charge components (the amount of air, fuel, and residual gas in the charge), fluid motion (large-scale motion and small-scale turbulence in the combustion chamber and their interaction with the flame), mixture

inhomogeneity (in charge composition and temperature), and spark discharge characteristics from one cycle to another [7].

Researchers agree that CCVs are higher in lean and highly diluted mixtures and at low loads (such as under idle conditions) [6, 7, 8, 9]. Hinze and Cheng [7] showed experimentally the influence of multiple factors in gasoline SI engines' CCVs at idle, showing that the indicated mean effective pressure (IMEP) fluctuations are mostly influenced by the variations in the flow field and charge inhomogeneity (54 %) and in the residual gas mass (around 33 %), while the variation of combustion durations are primarily caused by the flow field (around 80 %).

Truffin et al. [10] investigated the causes of cyclic variability experimentally and in LES simulations for a propane-fueled ICE. Their results show the rise of CCVs in diluted and lean mixtures. A multivariate analysis was done to evaluate the impacts of several parameters on the early flame and main propagation phases for both mixtures and then compared to the Ozdor et al. [6] experiments. For the early flame phase, the factor that was the most important for cyclic variability in the lean case was the flow field fluctuation, followed by the global dilution and equivalence ratio disparity, which supports Ozdor et al. main findings. However, flow field and global dilution impacts had a moderate correlation on the diluted mixture. For the main propagation phase, global dilution (and equivalence ratio, resp.) and in-cylinder charge impact moderately.

Nonetheless, hydrogen presents different properties compared to common fossil fuels, i.e. low density, low minimum ignition energy, broad flammability range, and intrinsic thermodiffusive instabilities. Since the combustion duration in an engine is related to the flame speed, hydrogen's broad flammability range (and equivalence ratio, consequently) impacts significantly the engine's combustion events [11, 12]. Hydrogen flame speed is a result of three main factors: the laminar flame speed, the turbulence level in the flow field, and the thermodiffusive instabilities [13, 14]; thus, research must be done to discern the influence of each of these factors on its flames and combustion durations in engines.

Many works have been done (mainly a decade ago) analyzing the effects of CCVs in H_2ICEs with both direct-injection (DI) and port fuel injection (PFI) systems [15, 16, 17, 18], but almost exclusively in gasoline baseline engines and with a close-to-stoichiometric mixture. Hydrogen-air equivalence ratio, engine speed, and load impacts on cyclic variations of gasoline baseline H_2ICEs were investigated. Kim et al. [15] concluded that the increase of CCVs with the decrease in the equivalence ratio depends primarily on the flame initiation process. Ma et al. [16] found that the instabilities increased with lower loads. Finally, Chen [17] studied the performance of PFI hydrogen-fueled engines at idling and concluded that hydrogen injection timing minimally affects CCVs, and Sun et al. [18] showed that ignition timing had great effects on CCVs, mainly at low equivalence ratios, being minimum at MBT.

At the moment, a great part of H_2ICE research is being done with existing diesel or gasoline baseline retrofitted engines [11]. These platforms have different working principles and, consequently, different characteristics, such as the displacement volume, the amount of heat transfer, and the structure of internal aerodynamics (level of turbulent motion at spark timing, for example). That is the reason why studies in both architectures must be done to assess hydrogen combustion properties and probable impacts of aerodynamics and injection type on combustion phenomena.

The present work is focused on the experimental analysis of hydrogen combustion and cyclic variations on diesel baseline retrofitted H_2ICEs. Its objectives are understanding ultra-lean/lean hydrogen combustion at low turbulent/swirling flow ICE architectures, which are not amply studied, and evaluating the key parameters affecting flame development and CCVs at these conditions. These insights could be helpful as a mid-term solution for the low-carbon economy by the adaptation of current diesel engines for hydrogen to promptly ease carbon emissions, and as a long-term solution, by providing experimental knowledge on hydrogen combustion and CCVs for the development of hydrogen-efficient architectures.

EXPERIMENTAL SETUP AND METHODOLOGY

Two four-cylinder converted to single-cylinder, four-stroke diesel baseline, engines were adapted for these experiments. Both engines have flat cylinder-head and bowl-type pistons. The first one is a DI light-duty, central injection, while the second one is a PFI medium-duty engine. A study was made to modify both engines' pistons. The compression ratio was adjusted for hydrogen combustion, optimizing stability and preventing knock at high loads. The bowl shape was maintained. Table 1 shows the test bench specifications.

For both engines, the cooling water is heated up to 88 °C and kept under 90 °C during all experimental conditions. The intake air is particle and oil filtered, dehumidified, and heated by an electric air pre-heater positioned upstream of the intake manifold. The intake and exhaust air temperatures and pressures are maintained constant by a closed-loop controller to represent real intake line conditions and exhaust line back pressure, respectively. Temperatures are measured by K-type thermocouples.

The engine parameters are adjusted by an in-house Lab-View engine control system. The exhaust gas components (O_2, CO, CO_2, HC, and NOx) are measured by a Horiba Mexa 7100D-EGR exhaust gas analyzer. The engine is coupled to an alternator and an electric engine that can ensure motoring operations from 600 to 1900 rpm. An optical encoder ensures the recording of 100 cycles with a 0.1 CAD increment. A Borg Warner CHG 6.2 injector provides an H_2 spray from a 30-bar circuit in both light-duty and medium-duty

Table 1: Engines' test bench specifications.

Engine test-bench	Light-Duty	Medium-Duty
Engine model	PSA DW10	Volvo MH8
Number of cylinders	Single-cylinder	
Architecture	Diesel baseline (retrofitted)	
Piston	Bowl type	
Injection type	DI	PFI
Displacement volume	0.5 L	1.28 L
Compression Ratio	12.7	12.4
Intake plenum volume	7 L	40 L
Exhaust plenum volume	3 L	40 L

engines. The injection is phased from -220 to -45 ^{o}aTDC and from 300 to -175 ^{o}aTDC at the light-duty DI and the medium-duty PFI engines, respectively, which means that the second one has a more homogeneous mixture in theory.

The light-duty engine, illustrated in Figure 1, has an AVL GH15D piezoelectric sensor to measure the in-cylinder pressure. Intake and exhaust pressures are obtained from Kistler 4075A piezoresistive sensors. Finally, the air and hydrogen mass flows are measured by two Coriolis mass flow meters: Micro Motion F025S and Micro Motion CMFS010. The hydrogen injector is located at the center of the combustion chamber.

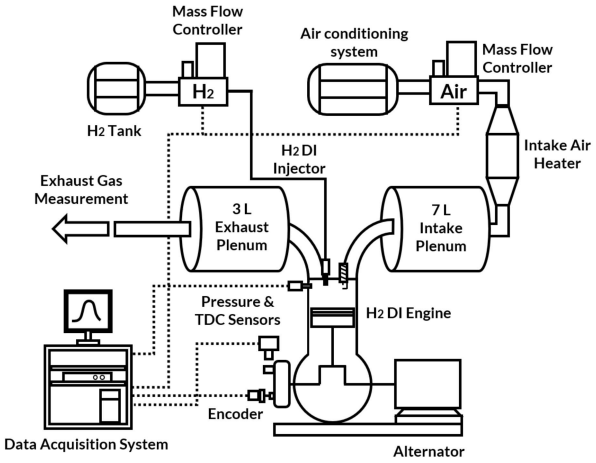

Figure 1: Light-duty DI hydrogen-fueled engine's experimental setup.

The medium-duty engine shown in the work from Oung et al. [19] has a similar experimental setup compared to the light-duty test bench, but with greater plenum volumes (40 L at both intake and exhaust) and hydrogen injector placed on the intake manifold. In-cylinder pressure is measured by a Kistler 6125CU20 piezoelectric sensor, and intake and exhaust pressures are obtained from Kistler 4075A piezoresistive sensors as well. Air and hydrogen mass flows are measured by Micro Motion CMFS025 and Micro Motion CMFS010 Coriolis mass flow meters, respectively. The hydrogen mass flow meters were calibrated for these studies. The lower precision in hydrogen measurement is 2 % of the measured value and it happens at low loads and hydrogen mass flows. At other operating conditions, the precision is 0.25 % of the measured value.

With these experimental setups, the effects of equivalence ratio, swirl intensity, load, and spark timing were evaluated on the light-duty engine, and the effects of equivalence ratio and spark plug type were studied on the medium-duty engine, as shown in Table 2.

Table 2: Experiments methodology (N.A. = Not applied).

Parameter	Light-Duty	Medium-Duty
Equivalence ratio	$0.3 < \phi < 0.7$	$0.2 < \phi < 0.8$
Swirl Intensity	Low, Normal, High	N.A.
Load	1, 3, 13 bar	N.A.
Spark timing	$5 < P_{ST} < 80$ bar	N.A.
Spark plug	N.A.	Cold, Semi-cold, Classic

For both configurations three key indicators of engine performance are analyzed, i.e. indicated mean effective pressure (IMEP), NOx emissions, and combustion duration ($\Delta\theta_{comb}$). The combustion duration ($\Delta\theta_{comb}$) of flame initiation (Ignition to 10 % of mass fraction burned – MFB), flame propagation (10 to 50 % of MFB), and end-flame (50 to 90 % of MFB) are separated. It is important to note that

since heat transfer models for hydrogen combustion are not yet fully developed [20], combustion parameters were calculated from the heat release with no heat transfer model.

To compute the CCVs, the coefficient of variation (CoV) of each parameter is calculated ($CoV_X = \sigma_X/\overline{X}$, where σ is the standard deviation of the X variable, and $\overline{X}$, its mean value over 100 cycles). The CoV_{IMEP}, the combustion duration ($\Delta\theta_{comb}$), and the CoV of these combustion durations ($\text{CoV}_{\Delta\theta_{comb}}$) are studied as indicators of engine stability, flame speed and combustion variability, respectively. Despite the common use of the standard deviation for the evaluation of combustion duration variability (with an absolute value of CAD), this work chose to investigate and represent combustion CCVs with the coefficient of variation because it illustrates the amount of deviation over the mean combustion duration (as a percentage). This helps to examine the combustion period variability independently from its duration. Otherwise, a combustion that takes a long time but does not exhibit great variability could have the same standard deviation value as another combustion whose duration is small but fluctuates a lot. Nevertheless, with the mean combustion duration values and their CoV, it is possible to recalculate the standard deviation for each combustion period by a simple multiplication.

Figure 2 illustrates examples of in-cylinder pressure and mass fraction burned (and their cyclic variations) for two different operating conditions in the light-duty engine as a function of the crank angle. The solid lines are the mean values over a hundred cycles and the shades are their standard deviation over the mean value. Both curves are representative of the same load (IMEP = 3 bar) with different intake pressures and equivalence ratios. The red line presents a mixture of ϕ = 0.39 and P_{int} = 0.70 bar, and the blue line, a mixture of ϕ = 0.54 and P_{int} = 0.55 bar.

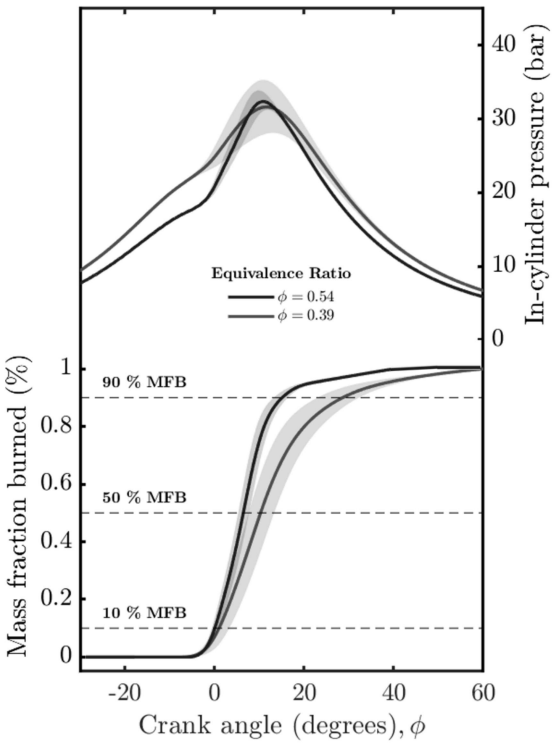

Figure 2: Cyclic variability of two operating conditions in the light-duty engine (low equivalence ratio - red - and high equivalence ratio - blue). Both operate at IMEP = 3 bar. Top: In-cylinder pressure trace. Bottom: mass fraction burned. The solid lines are the mean values over a hundred cycles and the shades are their standard deviation over the mean value.

The difference in CCVs and stability, at these two operating conditions, is clear. The pressure traces indicate that the cyclic variations, of the maximum pressure or the IMEP for example, are much higher in the red operating point (at a lower equivalence ratio) than in the blue one. The CoVs of IMEP for red and blue curves are 7.5 and 1.2 %, respectively, which quantify these fluctuations.

The mass fraction burned, which portrays the combustion progress, is different in both conditions as well. Total combustion is, as expected, faster at a higher equivalence ratio due to its higher flame speed. The CoV of the flame initiation duration ($\Delta\theta_{Ign.-10\%}$) for the low and high equivalence ratio conditions are 16.3 % and 11.3 %, respectively. The flame propagation (10 - 50 %) and the end-flame (50 - 90 %) are respectively 17.1 and 13.6 % for the low equivalence ratio and 11.5 and 9.9 % for the high equivalence ratio condition. These results indicate that both stability and combustion CCVs increase with a decrease in equivalence ratio at these conditions.

In the following section, the CoVs of IMEP and combustion durations are analyzed in every operating condition. Results are, then, discussed accounting for hydrogen flame properties.

RESULTS AND DISCUSSION

LIGHT-DUTY ENGINE

Effects of equivalence ratio: The fuel-air equivalence ratio is varied to understand its effects on diesel baseline H_2ICEs combustion.

Figure 3 shows the influence of the equivalence ratio on engine stability, NOx emissions, combustion duration, and combustion duration fluctuation at low loads (IMEP = 2 bar). The engine speed (950 rpm) and the start of injection – SOI (-140 °aTDC) – are maintained constant and CA50 is adjusted to MBT. The bottom graph illustrates the importance of the fuel-air equivalence ratio on IMEP variability and NOx emissions. It is logical that the closer the engine operates to stoichiometry, the higher NOx emissions are, with a maximum value of around 2500 ppm at ϕ = 0.7, and lower cyclic variations happen. On the contrary, lower equivalence ratios generate lower NOx and higher CCVs, which is in good agreement with known common fuel results [6, 10].

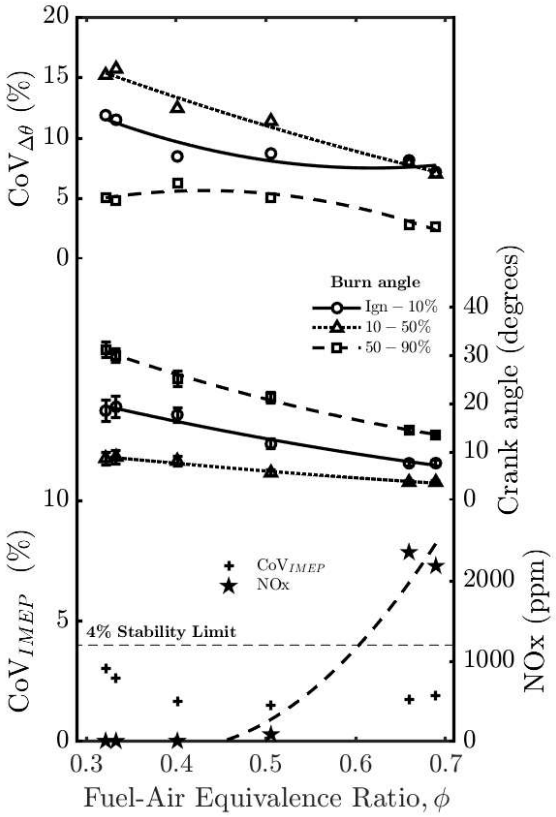

Figure 3: Effect of equivalence ratio on stability – CoV$_{IMEP}$ – and NOx emissions (bottom), combustion duration (middle) and combustion fluctuation – CoV$_{\Delta\theta}$ – (top) on the light-duty DI engine. Engine speed (950 rpm), the start of injection – SOI (-140 °aTDC) – and IMEP (2 bar) are maintained constant and CA50 is adjusted to MBT. The error bars are an indication of the standard deviation over a hundred cycles.

In the middle graph of Figure 3, one can observe the combustion duration of flame initiation, flame propagation, and end-flame as a function of the equivalence ratio. The error bars are an indication of the standard deviation over a hundred cycles. The second-degree trend lines indicate the combustion tendency, with a coefficient of determination (R^2) always greater than 97 %. It is possible to note that the end-flame period is the longest combustion duration, increasing from 14 CAD at ϕ = 0.7 to more than 30 CAD at ϕ = 0.3. The flame initiation process is the second longest combustion period and the flame propagation process is the fastest one, lower than 10 CAD in all equivalence ratios. Furthermore, combustion duration tends to increase with a low equivalence ratio, which seems to agree with the laminar flame speeds decrease at standard conditions. However, while the laminar flame speed is divided by ten (from ϕ = 0.65 to ϕ = 0.32) the combustion duration only increases by a factor of two (in all combustion periods).

The top graph of Figure 3 displays the cyclic variations of each combustion period as a function of the equivalence ratio. With it, it is possible to realize the impact of the equivalence ratio on the duration of each combustion period separately from its impact on the duration itself. The values in crank angle degrees can be analyzed on the middle graph with the standard deviation bars at each experimental point. The flame propagation period (10 to 50 % of MFB) is the one whose relative variation is the greatest: up to 15 % at ϕ = 0.3. Followed by the flame initiation period. This implies that the mixture's burn duration from 10 to 50 % of MFB, and consequently the flame speed, is highly dependent on what happened in the first stages of the flame, which results in higher combustion

variability, similar to what was found by Kim et al. [15] in gasoline baseline hydrogen engines. The end-flame period has the lowest variations, which in all conditions is less than 6 %. While the decrease in fuel-air equivalence ratio increases the cyclic variability of flame initiation and propagation at low loads, the end-flame duration does not seem to be much affected by it. This phenomenon means that the hydrogen combustion presents low variability from 50 % of the MFB independently from the variations that occurred before. This result could be explained by the fact that what rules the end-flame phase is the flow field, the heat transfer to the wall, and the flame quenching, which could be similar, at a specific condition, independently from the variation of initial conditions and the path of combustion events.

Effects of swirl intensity: In order to understand the effects of swirl intensity on hydrogen combustion, three different intakes architectures were tested, leading to low, normal, and high swirl levels at IMEP = 13 bar and SOI = -130 ^{o}aTDC. The DW10 nominal swirl ratio is 2 at the TDC (with the original piston). The normal swirl is defined as the condition without any modification. The intake geometry of this engine is characterized by two intake ports: a helical high-swirl port and a directed low-swirl port. For the high-swirl intensity condition, the intake system was modified so that intake gases are admitted exclusively by the helical high-swirl duct and valve. For the low swirl intensity, the intake gases are admitted exclusively by the directed low-swirl duct and valve. The equivalence ratio was also varied to apprehend its effect on swirl intensity results. For all operating points, engine performance was kept stable (under 4 % of CoV_{IMEP}).

In Figure 4, it is possible to see in the bottom graph that combustion duration increases independently to swirl intensity as the fuel-air equivalence ratio decreases. Moreover, one can see that the flame initiation process will be faster in a high-intensity swirl and slower in a low-intensity swirl, which could be explained by the fact that a greater mean velocity in the cylinder allows the flame kernel to move away from the spark plug region (since it is not centralized in the combustion chamber), lowering heat transfer with the spark plug and expanding more rapidly, as seen in propane combustion in Truffin et al. LES simulations [10]. Differently from common fuels [21], the end-flame period of normal intensity is higher than in high and low swirl configurations. The cyclic variations in combustion periods on the top graph, however, do not indicate a relation between cyclic variations in combustion and swirl intensity at these conditions. It is noteworthy that this engine architecture is different from the other ones studied previously since it is spark-ignition combustion on a low turbulence baseline (diesel engine architecture with flat cylinder-head). Consequently, the known conclusions, about increasing tumble motion intensity and decreasing cyclic variations as well as greater CCVs in the flame initiation phase [21], cannot be applied here.

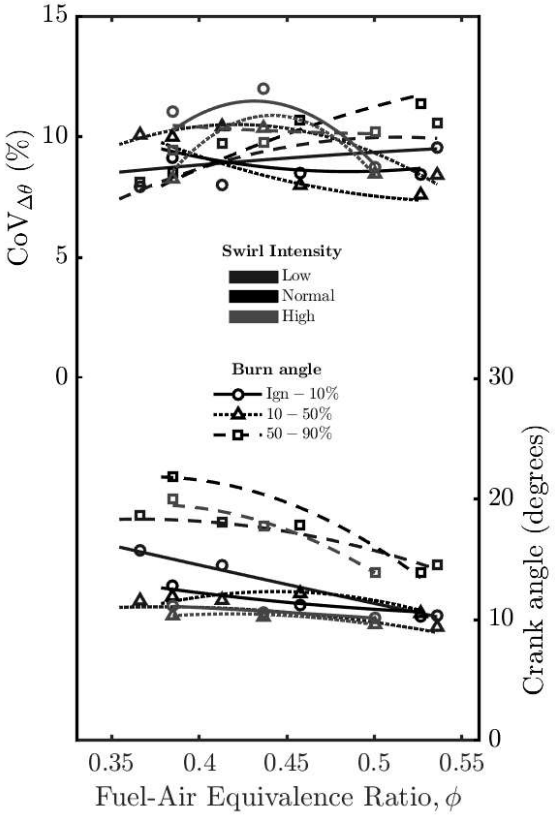

Figure 4: Effect of swirl intensity on combustion duration (bottom) and combustion fluctuation (top) on the light-duty DI engine. Engine speed (2000 rpm), SOI (-130 °aTDC), and IMEP (13 bar) are maintained constant.

Effects of load: Regarding the load effect on cyclic variability in a low-turbulence architecture, an experiment was done with three different targeted IMEPs: 1, 3, and 13 bars. The engine speed was kept constant for each IMEP (900, 1500, and 2000 rpm, respectively), and SOI was always at -140 °aTDC. Spark timing and equivalence ratio were varied to maintain a targeted CA50.

Figure 5 exhibits the CoV of IMEP, combustion durations, and combustion durations fluctuations as a function of the equivalence ratio. The bottom graph indicates the equivalence ratio range for the three different IMEPs. It is noteworthy that low loads were obtained with low equivalence ratio mixtures. At these conditions, the CoV_{IMEP} is higher, as is the case for common fuel engines [6]. On the contrary, with high loads operating conditions, the air management system provided was coupled with higher equivalence ratio mixtures to allow the demanded high power outputs. At these settings, the engine tends to have stable functioning.

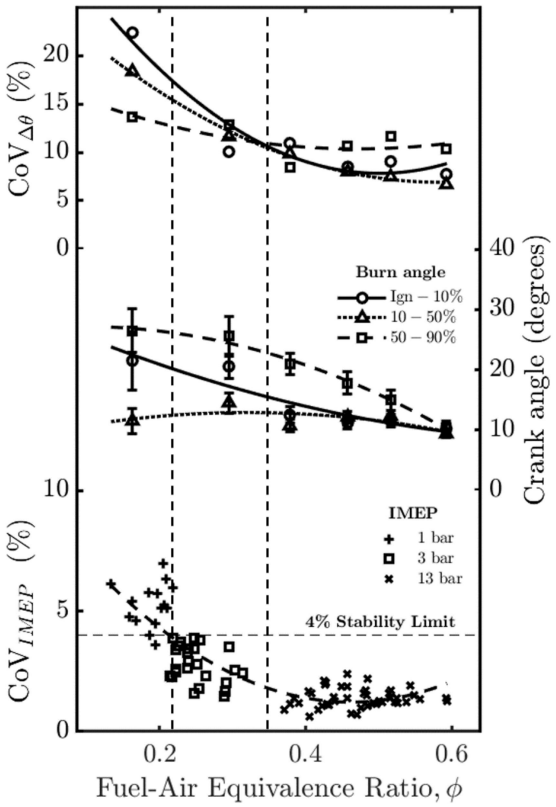

Figure 5: Effect of load on stability (bottom), combustion duration (middle), and combustion fluctuation (top) on the light-duty DI engine. For each targeted IMEP (1, 3, and 13 bar, separated by the dashed lines), engine speed (900, 1500, and 2000 rpm, resp.), SOI (-140 °aTDC) and intake pressure (0.7, 1, and 2.2 bar, resp.) are maintained constant. The error bars are an indication of the standard deviation over a hundred cycles.

The middle graph in Figure 5 presents the effect of load (and equivalence ratio) on hydrogen combustion in the cylinder. The points were filtered so the graph could be readable and the standard deviation over a hundred cycles is exhibited by error bars. The second-degree trend lines from experimental data indicate the combustion tendency ($R^2 > 50$ %). Interestingly, the flame propagation period presents the same duration in all engine loads, independently from the equivalence ratio. It is the fastest combustion period, followed by flame initiation and end-flame in all of these operating conditions. At higher loads, the combustion phases have almost the same duration. At low loads (IMEP = 3 bar), flame initiation and end-flame periods are longer than the flame propagation process. At this point, the end-flame duration takes about two times longer than the flame propagation period. Finally, at idle conditions, flame initiation takes even longer, approaching end-flame duration (which has a stagnation trend).

The combustion cyclic variability is displayed in the top graph of Figure 5. When the combustion CCVs are evaluated at higher loads, combustion duration variability for all phases is similar and around 10 % of the mean duration value. At lower loads, end-flame CCVs are maintained at the same order of magnitude, but both flame initiation and flame propagation fluctuations increase. At idle, this rise is even bigger. It is good to note that flame initiation is the phase that has the most cycle disparity and that even if the flame propagation undergoes the same duration over the different loads (and equivalence ratios), its cyclic variability does not follow this trend.

Effects of pressure at spark timing: The same experiment detailed before is now analyzed as a function of the pressure at spark timing. It is important to have in mind that at idle, the equivalence ratios are between 0.16 and 0.22; at low loads, they go from 0.22 to 0.35; and at high loads, they are between 0.35 and 0.6.

The bottom graph in Figure 6 displays the combustion durations as a function of the pressure at spark timing. The experimental points are filtered for the clarity of the graph and the trend lines are added ($R^2 > 50\%$). From this, it is possible to see that the combustion durations are not that impacted between these three loads. The order of magnitude is the same, even if the laminar flame speeds at these conditions are meant to be an order of magnitude different. Moreover, it must be recalled that the change of spark timing and equivalence ratio are simultaneous, thus their effects are coupled in the experimental results. The same effect of differing combustion duration as the load reduces is observed. While higher pressures at spark timing (and equivalence ratio, as well) lead to similar combustion durations for the flame initiation and propagation periods and the end-flame between 1.2 to 2 times higher, low pressures accentuate the difference of flame initiation and end-flame from flame propagation (1.8 and 2.5 times greater at idle, respectively). Another interesting result is the fact that flame initiation and end-flame durations become close to one another as the pressure at spark timing becomes small (at low loads and idle conditions).

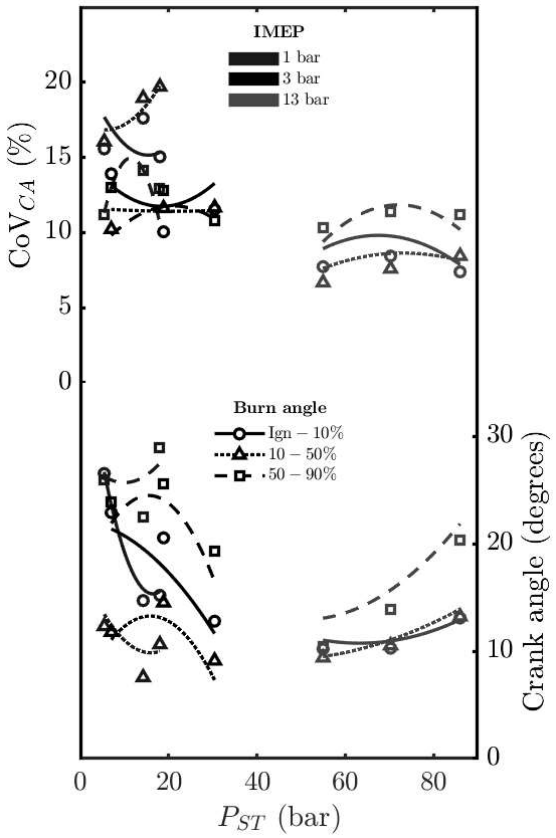

Figure 6: Effect of pressure at spark timing on combustion duration (bottom) and combustion fluctuation (top) on the light-duty DI engine. For each targeted IMEP (1, 3, and 13 bar, separated by the dashed lines), engine speed (900, 1500, and 2000 rpm, resp.), SOI (-140 °aTDC) and intake pressure (0.7, 1, and 2.2 bar, resp.) are maintained constant.

Finally, the top graph of Figure 6 shows the influence of the in-cylinder pressure at spark timing on combustion periods' CCVs. As seen previously, cyclic variations of the end-flame period are alike in the three different loads, not changing much with pressure and equivalence ratio, which could be an effect of the end-flame properties mentioned earlier. Moreover, both flame initiation and propagation durations' CCVs raise considerably with the load. At idle conditions, flame initiation and propagation fluctuations can be as high as 18 and 20 %, respectively. This result diverges from the Hinze et al. [7] gasoline engine experiments at idle, in which the end-flame was the period with the most fluctuations, affected mainly by the flow field variations. The pressure at spark timing in the same load condition, however, does not have a clear impact on combustion CCVs. The pressure spark timing's variation at 13 bar of IMEP, for instance, from 50 to 90 bar did not have an impact on the CCVs, which remained around 9 %. The same can be said for IMEPs of 3 bar, whose values are about 11 %. The CCVs at low loads are more dispersed, but between 10 and 20 %.

MEDIUM-DUTY ENGINE

Effects of equivalence ratio: The effects of the equivalence ratio were also observed in a medium-duty PFI engine. Its' displacement volume is almost three times greater than the one analyzed previously, and hydrogen/air mixtures are theoretically more homogeneous since the injection is done at the intake manifold. The test is performed at medium load (IMEP = 10 bar).

Figure 7 shows the influence of the equivalence ratio on engine stability and NOx emissions, combustion duration, and combustion periods' fluctuation. It is possible to note, at the bottom graph, that as the equivalence ratio is higher, NOx emissions are greater (more than 4000 ppm - in volume - at $\phi = 0.7$) and stability is better (less than 2 % of CoV_{IMEP} at $\phi = 0.6$), also shown in Figure 3, which can be explained by the higher flame temperatures at higher equivalence ratios. On the contrary, an equivalence ratio of less than 0.5 reduces considerably NOx emissions, and less than 0.3 decreases engine stability.

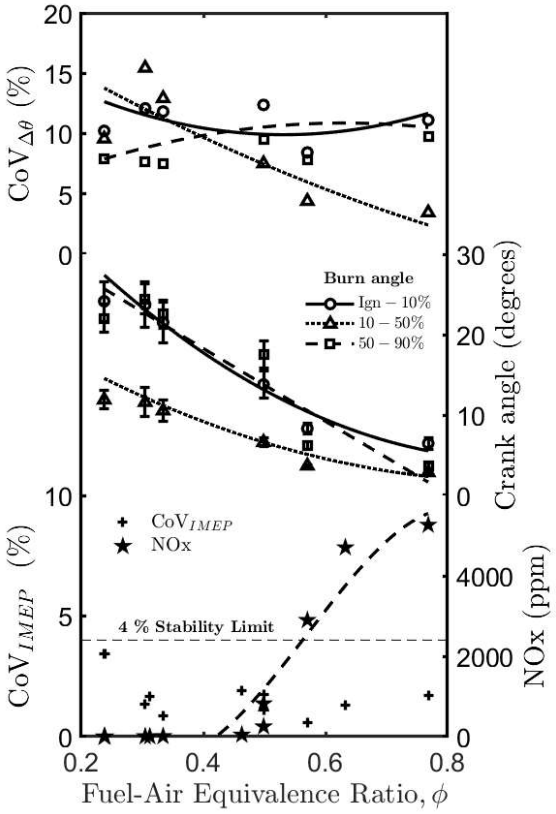

Figure 7: Effect of equivalence ratio on stability (bottom), combustion duration (middle), and combustion fluctuation (top) on the medium-duty PFI engine. Engine speed (900 and 1400 rpm), the start of injection – SOI (-350 °aTDC) – and IMEP (10 bar) are maintained constant. The error bars are an indication of the standard deviation over a hundred cycles.

The middle graph of Figure 7 displays the combustion durations of flame initiation, propagation, and end-flame as a function of the equivalence ratio. At these conditions; flame propagation is the fastest combustion phase, and flame initiation and end-flame combustion have similar values and trends under $\phi = 0.6$.

In regards to the CCVs of the three combustion phase durations, the top graph of Figure 7 illustrates that both flame initiation and end-flame durations fluctuations are not much impacted by the equivalence ratio sweep, remaining around 10 %. The flame propagation duration, however, is highly impacted by this variation, passing from less than 5 % of $\mathrm{CoV}_{\Delta\theta_{10-50\%}}$ to about 15 %.

When one observes the impact of the equivalence ratio sweep in the flame propagation duration CCV in both engines, it is clear that this combustion phase is the most impacted. As seen in Figures 3, 5, and 7, the combustion duration is not exclusively driven by the laminar flame speed property of hydrogen. When one compares it with the combustion durations, no linear relation is observable. So, another factor impacts flame development together with the laminar flame speed property, as mentioned before.

To take into account the influence of the intrinsic instabilities in hydrogen-premixed flames, such as the flame front wrinkling and the variations of reaction rates, an integral measure of flame speed, named consumption speed s_C, is used. This flame speed indicator considers that an unstable flame can have a significantly higher flame speed compared to planar, unstretched laminar flames. The correlation of Berger et al. [13], in Equation 1, is used to add the effects of equivalence ratio, unburned temperature, and pressure on the thermodiffusive instabilities.

$$\frac{\left(\frac{s_C}{s_L}\right) - 1}{\left(\frac{s_C}{s_L}\right)_{Ref} - 1} = \left(\frac{\phi}{\phi_{Ref}}\right)^{\gamma_\phi} \left(\frac{T_u}{T_{u,Ref}}\right)^{\gamma_{T_u}} \left(\frac{p}{p_{Ref}}\right)^{\gamma_p} \tag{1}$$

Where s_L is the laminar flame speed, T_u is the unburned gas temperature, p is the pressure and the γs are the scaling coefficients for each ratio (equivalence ratio, unburned temperature, and pressure) found in their studies. The reference case conditions and the exponents are the following: $\left(\frac{s_C}{s_L}\right)_{Ref}$ = 2.70, ϕ_{Ref} = 0.5, $T_{u,Ref}$ = 298 K, p_{Ref} = 1 bar, γ_ϕ = -1.62, γ_{T_u} = -2.56 and γ_p = 0.40.

Figure 8 shows the consumption speed - laminar flame speed ratio, s_C/s_L, and the consumption speed as a function of the equivalence ratio in the light-duty engine. The consumption speed was calculated with pressure and temperature data at the spark timing.

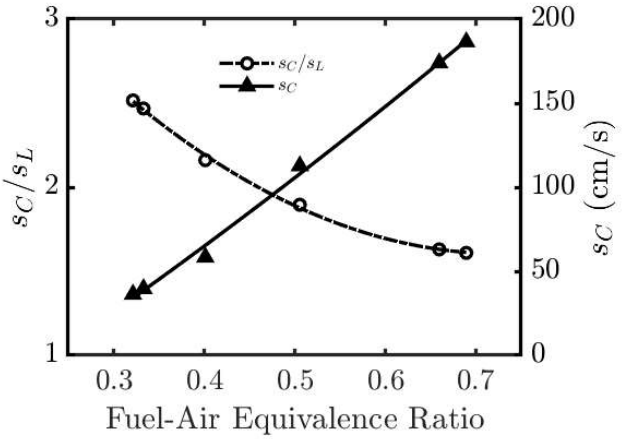

Figure 8: Effect of the equivalence ratio on the ratio s_C/s_L and the consumption speed in the light-duty DI engine. The operating conditions are the same as in Figure 3. The flame speed is calculated from the Berger et al. correlation [13] at spark timing conditions.

The s_C/s_L ratio displays the accelerating nature of the intrinsically unstable flame. It is higher at leaner mixtures, being almost 1.6 times greater comparing ϕ = 0.32 and ϕ = 0.69.

In addition, the consumption speed, differently from the laminar flame speed, presents a linear dependency on the equivalence ratio. This behavior is also found in the combustion duration for these operating conditions, in Figure 3. This means that, differently from the laminar flame speed, the consumption speed is directly correlated with the combustion durations in these H_2ICE conditions.

To analyze this effect, Figure 9 plots combustion durations and combustion duration CCVs as a function of the hydrogen consumption speed. The bottom graph indicates the enhancement of the flame speed when one takes into account the flame instabilities and their linear impact on combustion durations.

In the top graph, one can also observe the linear impact of consumption speed on flame propagation fluctuations. However, the end-flame and flame initiation fluctuations do not present the same behavior. While the end-flame CCV does not seem to be influenced by the flame speed (and equivalence ratio), the flame initiation fluctuation does not seem to be impacted at higher equivalence ratios but shows high impacts at lower equivalence ratios.

Effects of spark plug type: The last experiment is done by varying the spark-plug type for four conditions with IMEP values of 1, 13, and 15 bar in order to understand the impact of spark plugs in combustion and CCVs. The spark plugs used are named ”classic” (hot), ”semi-cold”, and ”cold” related to their heat range references (NGK Heat Range of 7, 8, and 11, respectively).

Table 3 indicates the CoV of IMEP for the operating conditions. In general, ”hotter” spark plugs produce higher stability. This result is clearer at low loads, where ”colder” spark plugs generate much higher cyclic variations (leading even to a misfire in ϕ = 0.16). At high loads, the difference in stability between the different types of spark plugs is less apparent. However, under these conditions knock starts to appear more frequently with classic spark plugs.

Table 3: Spark plug type impact on CoV_{IMEP} (%).

Spark plug type	**1 bar***	**1 bar****	**13 bar**	**15 bar**
Classic (Hot)	10.1	5.6	0.85	0.6
Semi-cold	23.2	6.2	1.2	0.5
Cold	>100***	5.7	1.5	0.7

* ϕ = 0.17 and P_{int} = 0.9 bar.
** ϕ = 0.21 and P_{int} = 0.7 bar.
*** misfire

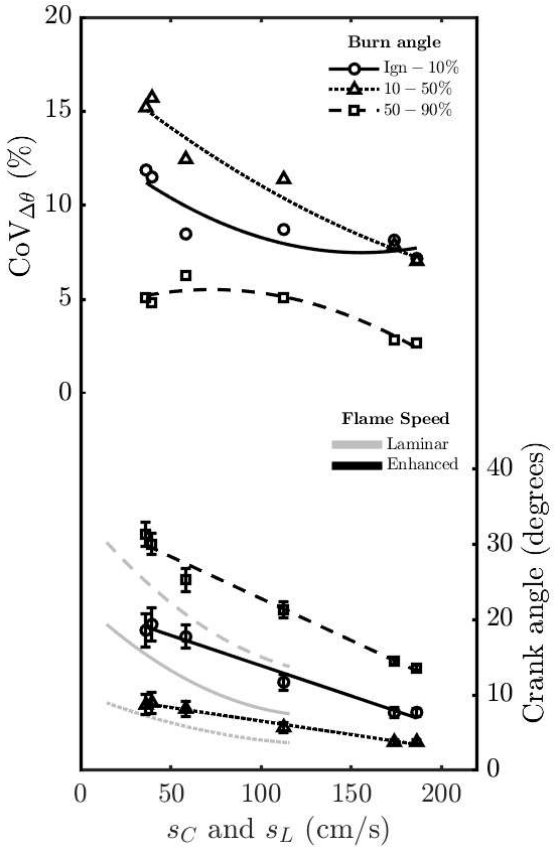

Figure 9: Effect of hydrogen flame speed on combustion duration (bottom) and combustion fluctuation (top) on the light-duty DI engine. The operating conditions are the same as in Figure 3. The flame speed is calculated from the Berger et al. correlation [13] at spark timing conditions. The linear trend line for combustion duration with the consumption speed ($R^2 > 98$ %), the second-degree trend line for combustion duration with the laminar flame speed ($R^2 > 99$ %), and the second-degree trend line for combustion CCVs ($R^2 > 78$ %).

Table 4 indicates the maximum knock intensity (in bar), calculated as the maximum amplitude of the high-pass filtered pressure signal, for high load conditions. A direct comparison can be made between "hotter" spark plugs and higher maximum knock intensities.

Table 4: Spark plug type impact on maximum knock intensity (bar).

Spark plug type	**13 bar**	**15 bar**
Classic (Hot)	1.07	0.76
Semi-cold	0.85	0.23
Cold	0.60	0.48

CONCLUSION

Experiments were done in two diesel baseline hydrogen-fueled internal combustion engines. Stability, NOx emissions, combustion durations, and flame phases' fluctuations were analyzed in a low-turbulence architecture by varying equivalence ratio, swirl intensity, load, spark timing and spark plug types. The results were analyzed and compared to hydrogen flame's fundamental properties. The main conclusions that can be drawn from this work are stated below:

- As in gasoline baseline engines, low equivalence ratios and loads in a diesel baseline H_2ICE lead to higher combustion durations and cycle-to-cycle variations.
- Swirl intensity is responsible for a faster (high swirl) or a slower (low swirl) flame initiation phase. Possibly due to the convection of the flame kernel, lowering heat transfer, and quenching effects. Other combustion phases were not affected by it. Furthermore, swirl intensity presents no apparent effect on combustion cyclic variations.
- In-cylinder pressure at the spark timing does not have a direct influence on combustion CCVs. A variation of 5 to 30 bar at 3 bar of IMEP did not change the combustion durations CoVs (around 11 %), so as the variation of 50 to 90 bar at 13 bar of IMEP (CoVs around 9 %).

- Spark plug choice is important in hydrogen-fueled internal combustion engine development. Hotter spark plugs (in use on common fuels engines) produce fewer CCVs but could be a hot spot for abnormal combustions, due to hydrogen's low minimum ignition energy and broad flammability range. A compromise must be done between having fewer CCVs (classic spark plugs) and avoiding abnormal combustions (colder spark plugs).
- The combustion phase the most affected by CCV with equivalence ratio sweep is the flame propagation. This increase in fluctuations could be provoked by the levels of flame wrinkling which depends on temperature, pressure, and equivalence ratio at the vicinity of the spark plug during the flame initiation phase. Further studies must be done to strengthen this physical analysis of the results.
- The consumption speed (with the thermodiffusive instabilities accounted for) was found to be better related to the combustion durations in H_2ICEs than the laminar flame speed property.

The current study investigated the effects of parameter variation on engine stability, combustion duration, and combustion fluctuations. Additional diagnostics in optically accessible engines evaluating flame development and in-cylinder motion, and targeted numerical LES simulations, focusing on H_2ICEs cyclic variation causes, are subjects of future work.

ACKNOWLEDGEMENTS

The generous support of the Agence Nationale de Recherche under grant number 20-CE05-0007 (ALEKCIA ANR project) is gratefully acknowledged.

REFERENCES

[1] P. Shukla, J. Skea, R. Slade, A. A. Khourdajie, R. van Diemen, D. McCollum, M. Pathak, S. Some, P. Vyas, R. Fradera, M. Belkacemi, A. Hasija, G. Lisboa, S. Luz, and J. Malley, "Working group iii: Mitigation of climate change," *Sixth Assessment Report of the Intergovernmental Panel on Climate Change*, 2022.

[2] F. Lévêque, J.-M. Glachant, J. Barquin, C. von Hirschhausen, F. Holz, and W. J. Nuttall, *Security of Energy Supply in Europe. Natural Gas, Nuclear and Hydrogen*. Edward Elgar, 2010.

[3] D. G. Caglayan, H. U. Heinrichs, M. Robinius, and D. Stolten, "Robust design of a future 100% renewable european energy supply system with hydrogen infrastructure," *International Journal of Hydrogen Energy*, vol. 46, no. 57, pp. 29376–29390, 2021.

[4] S. Verhelst and T. Wallner, "Hydrogen-fueled internal combustion engines," *Progress in Energy and Combustion Science*, vol. 35, no. 6, pp. 490–527, 2009.

[5] M. B. Young, "Cyclic dispersion in the homogeneous-charge spark-ignition engine — a literature survey," in *SIA Transactions*, vol. 90, pp. 49–73, 1981.

[6] N. Ozdor, M. Dulger, and E. Sher, "Cyclic variability in spark ignition engines - a literature survey," *SAE Technical Papers*, no. 940987, 1994.

[7] P. C. Hinze and W. K. Cheng, "Assessing the factors affecting si engine cycle-to-cycle variations at idle," in *International Symposium on Combustion*, vol. 27, pp. 2119–2125, 1998.

[8] R. K. Maurya and A. K. Agarwal, "Experimental investigation on the effect of intake air temperature and air–fuel ratio on cycle-to-cycle variations of hcci combustion and performance parameters," *Applied Energy*, vol. 88, no. 4, pp. 1153–1163, 2011.

[9] B. Deng, K. Hou, X. Duan, and Z. Xu, "The correlation between intake fluctuation and combustion ccv (cycle-to-cycle variations) on a high speed gasoline engine: A wide range operating condition study," *Fuel*, vol. 304, no. 121336, 2021.

[10] K. Truffin, C. Angelberger, S. Richard, and C. Pera, "Using large-eddy simulation and multivariate analysis to understand the sources of combustion cyclic variability in a spark-ignition engine," *Combustion and Flame*, vol. 162, no. 12, pp. 4371–4390, 2015.

[11] Z. Stepien, "A comprehensive overview of hydrogen-fueled internal combustion engines: Achievements and future challenges," *Energies*, vol. 14, no. 20, 2021.

[12] G. A. Karim, "Hydrogen as a spark ignition engine fuel," *International Journal of Hydrogen Energy*, vol. 28, no. 5, pp. 569–577, 2003.

[13] L. Berger, A. Attili, and H. Pitsch, "Intrinsic instabilities in premixed hydrogen flames: parametric variation of pressure, equivalence ratio, and temperature. part 2 – non-linear regime and flame speed enhancement," *Combustion and Flame*, vol. 240, p. 111936, 2022.

[14] L. Berger, A. Attili, and H. Pitsch, "Synergistic interactions of thermodiffusive instabilities and turbulence in lean hydrogen flames," *Combustion and Flame*, vol. 244, p. 112254, 2022.

[15] Y. Kim, J. T. Lee, and G. H. Choi, "An investigation on the causes of cycle variation in direct injection hydrogen fueled engines," *International Journal of Hydrogen Energy*, vol. 30, no. 1, pp. 69–76, 2005.

[16] F. Ma, H.-Q. Liu, Y. Li, Y. Wang, and S.-L. Zhao, "Analysis of in-cylinder combustion of hydrogen fueled engine," *Chinese Internal Combustion Engine Engineering*, vol. 29, pp. 29–33, 2008.

[17] Y. Chen, "Stability research of hydrogen internal combustion engine in idle condition," master's thesis, Beijing Institute of Technology, 2008.

[18] B. Sun, D. Zhang, and F. Liu, "Cycle variations in a hydrogen internal combustion engine," *International Journal of Hydrogen Energy*, vol. 38, no. 9, pp. 3778–3783, 2013.

[19] R. Oung, F. Foucher, J.-M. Neveu, A. Vucher, and E. Resier, "H2 efficient and near zero emissions operation on a pfi hd single cylinder diesel ice," in *SIA Powertrain & Energy*, Rouen, 2022.

[20] J. Demuynck, M. De Paepe, H. Huisseune, R. Sierens, J. Vancoillie, and S. Verhelst, "On the applicability of empirical heat transfer models for hydrogen combustion engines," *International Journal of Hydrogen Energy*, vol. 36, no. 1, pp. 975–984, 2011. 11th International Conference: "Hydrogen Materials Science & Chemistry of Carbon Nanomaterials".

[21] P. Hill and D. Zhang, "The effects of swirl and tumble on combustion in spark-ignition engines," *Progress in Energy and Combustion Science*, vol. 20, no. 5, pp. 373–429, 1994.